

# Effects of Vein Structures on Fluid-structure Interaction of Flexible Flapping Wings at High Altitudes

Madhu K. Sridhar<sup>1</sup>, Jeremy Pohly<sup>1</sup>, Chang-kwon Kang<sup>2</sup>, David Brian Landrum<sup>3</sup>

University of Alabama in Huntsville, Huntsville, AL 35899

Taeyoung Lee<sup>4</sup>

George Washington University, Washington, DC, 20052, USA

# Hikaru Aono<sup>5</sup>

Shinshu University, Ueda, Nagano, 386-8567, Japan

The long-range migration of monarch butterflies, extending over 4000 km, is not well understood. Monarch butterflies have large flexible wings which deform significantly during flight. Monarchs also experience varying air density conditions during their highaltitude migration and overwintering. In this study, we report the effects of different vein structural models and chordwise elastic modulus on the aerodynamic performance of monarch butterfly scale flexible wings. A well-validated, fully-coupled Navier-Stokes and structural dynamics model is solved to illustrate the interplay between the wing motion, aerodynamics, and structural flexibility in forward flight. In general, the lift and thrust magnitudes increase with the wing stiffness and stroke plane angle. For softer wings, the force magnitudes depend on the air density and decrease with the altitude. The power consumption increases with the stiffness. The monarchs can produce sufficient lift to fly by increasing the stroke plane angle in thin air at the migration and overwintering altitudes. The thrust and power consumption are small. At these higher altitudes, the monarchs may be operating in an energy efficient mode by utilizing their flexible wing structures. At the sea-level, the thrust is larger, implying that the monarchs can climb and rapidly accelerate at the cost of increased power. Our results suggest bioinspired micro flight vehicles can benefit from using flexible wings to passively modulate the aerodynamic force generation and save power consumption for highly efficient long-range flight.

#### **Nomenclature**

 $C_{\rm L} = {\rm coefficient\ of\ lift}$  [1]  $C_{\rm L,excess} = {\rm excess\ lift\ coefficient}$  [1]  $c_{\rm m} = {\rm mean\ wing\ chord}$  [m]

<sup>&</sup>lt;sup>1</sup> Graduate Student, Mechanical and Aerospace Engineering, Technology Hall C200, AIAA Student Member.

<sup>&</sup>lt;sup>2</sup> Associate Professor, Mechanical and Aerospace Engineering, Technology Hall N266, AIAA Senior Member.

<sup>&</sup>lt;sup>3</sup> Associate Professor, Mechanical and Aerospace Engineering, Technology Hall N267, AIAA Associate Fellow.

<sup>&</sup>lt;sup>4</sup> Professor, Department of Mechanical and Aerospace Engineering, SEH 3610.

<sup>&</sup>lt;sup>5</sup> Associate Professor, Department of Mechanical Engineering and Robotics, AIAA Member.

$C_{\mathrm{P}}$	=	coefficient of power input	[1]
$C_{\mathrm{T}}$	=	coefficient of thrust	[1]
E	=	chordwise elastic modulus	[Pa]
f	=	flapping frequency	[1/s]
$f_1$	=	first natural frequency of the wing	[1/s]
$f/f_1$	=	frequency ratio	[1]
F	=	fluid force acting per unit length	[N/m]
$F_{\rm lin}$	=	applied force in FEM	[N]
$h_{\perp}$	=	plunge motion	[m]
h	=	plunge velocity	[m/s]
$h_{\rm a}$	=	plunge amplitude, $h_a = \gamma_{p2p} R \hat{r}_2 / 4$	[m]
$h_{\mathrm{s}}$	=	membrane thickness	[m]
$h_{\rm s}$	=	thickness ratio, $h_s^* = h_s/c_m$	[1]
k	=	reduced frequency, $k = \pi f c_m / U$	[1]
L	=	lift	[N]
$m_{ m w}$	=	butterfly forewing mass	[kg]
m	=	total butterfly mass	[kg]
$\stackrel{oldsymbol{P}}{\hat{}}$	=	power (P)	[W]
$\hat{r}_2$	=	non-dimensional radius to the second moment of wing area, $\hat{r}_2 = r_2/R$	[1]
R	=	wing length	[m]
Re	=	Reynolds number, $Re = \rho_f U c_m / \mu$	[1]
S St	=	wing area Strouhal number, $St = 2fh_a/U$	$[m^2]$
T	=	thrust	[1] [N]
t	=	time	[s]
$t^*$	=	non-dimensional time	[5] [1]
U	=	freestream velocity	[m/s]
$\ddot{w}$	=	trailing edge vertical acceleration	$[m/s^2]$
$W_{\rm b}$	=	Average butterfly weight	[N]
α	=	pitch angle	[deg]
	=	pitch amplitude	[deg]
$\alpha_a$	=	end-of-stroke passive pitch angle	[deg]
$\alpha_{\rm e}$	=	effective angle of attack	[deg]
$lpha_{ m eff}$	=	mid-stroke passive pitch angle	[deg]
$\alpha_{\rm m}$	=	stroke plane angle	
β	=	peak to peak flapping amplitude	[deg]
γ <sub>p2p</sub>	=	deflection	[deg]
δ	=		[m]
ф		phase offset between pitch and plunge motion	[deg]
$ ho_{ m f}$	=	air density	$[kg/m^3]$
$\rho_{s}$	=	structural density of wing	$[kg/m^3]$
$ ho^*$	=	density ratio, $\rho^* = \rho_s/\rho_f$	[1]
μ	=	dynamic viscosity coefficient	[kg/(m-s)]

# I. Introduction

MIGRATION of monarch butterflies is the longest among insects. Each year hundreds of millions of monarch butterflies fly 4000 km during the fall [1–3]. This incredible journey interests many scientists and remains a mystery even to this day. The physical understanding of the aerodynamic mechanism behind long range migration of monarchs is currently underexplored.

During migration, glider pilots have spotted monarch butterflies at altitude up to 1200 m [4]. At these high altitudes in the boundary layer of the earth, the monarch can take advantage of favorable weather and wind patterns [3,5,6], presumably to conserve energy [7,8]. Additionally, all of their overwintering sites in Mexico are located at altitudes between 2900 m and 3200 m [9–13]. This high-altitude forest ecosystem is believed to lower the monarch's metabolic rates [3,14].

At an altitude of 3000 m, the air density  $\rho_f$  is about 76 % the density at sea level [15]. At these higher altitudes, monarchs experience reduced aerodynamic drag forces due to lower air density, which can help in long-range flight. However, the reduced density at high altitudes should also reduce the aerodynamic lift which is required to stay aloft. The lift generation mechanism in monarchs essential for high-altitude long-range flight of monarchs is also inadequately understood.

One of the main effects of flying in a lower density environment is that the operating Reynolds number reduces. Monarch butterflies in general operate at Reynolds number  $Re = \rho_f U c_m / \mu = O(10^3)$ , based on the reference velocity U, average wing chord length  $c_m$ , and dynamic viscosity of air  $\mu$ . In our recent free flight measurements of monarch butterflies at simulated altitudes, the Reynolds number was Re = 3326, based on average thorax velocity and mean chord length of considered butterfly specimens and air density of  $\rho_f = 1.2 \text{ kg/m}^3$ .

Another effect of the varying air density on the flight of monarchs is the fluid-structure interaction (FSI) of the flexible wings. Monarch butterflies have a large pair of wings compared to their body size [16]. The large wings have anisotropic structural material properties and undergo significant deformation during flight. The anisotropic nature of the wings arises from the combination of branching veins interlaid with membranes and material anisotropy [16]. Flexural stiffness of insect wings varies differently along the spanwise and chordwise directions [17]. Typically, the chordwise wing stiffness is significantly lower (i.e. more flexible) and directly affects aerodynamic performance through effective angle of attack, resulting in increased load lifting capabilities [18]. Compliant wings are also shown to contribute in power reduction [19–22]. For example, wing deformations of locusts and hawkmoths have been shown to enhance the force generation and improve aerodynamic efficiency [23–25]. One of the key non-dimensional parameters characterizing the FSI of flapping wings is the density ratio  $\rho^* = \rho_s/\rho_f$ , the ratio between the structural density of the wing  $\rho_s$  and the surrounding fluid density  $\rho_f$ . The fluid density changes from 1.2 kg/m³ to 0.909 kg/m³ between 193 m and 3000 m which is the overwintering altitude of monarchs. The coupled interaction of the reduced density of the surrounding fluid and the structural characteristics of the anisotropic wing affects the FSI of the monarch wings.

In our previous work [26], we investigated the aeroelastic response of the monarch wings at high altitudes. Based on a micro-CT scan image of a monarch wing, we conducted an finite element modeling (FEM) analysis in the chordwise direction [16]. The resulting elastic modulus was 0.2 GPa. We used a well-validated, fully-coupled FSI framework [22,27–31] to solve the Navier-Stokes equations for the flow around a two-dimensional cross-section of a monarch scale wing, modeled as a beam. We investigated the effects of the varying density on the resulting aerodynamic performance. Our results showed that mean lift reduced with altitude but increased with stroke plane angle. The power required decreased with altitude. At the overwintering altitude of 3000 m, the wing generated sufficient lift by changing the stroke-plane angle to 50 deg.

However, our experimental measurements from free flights recorded between altitudes of 193 m and 4500 m, simulated by reducing the air density in a vacuum chamber, indicated that the stroke-plane angle varied between 3.3 deg [26]. This discrepancy in the stroke plane angle may be due to the way the vein structure was modeled in our previous work [16]. In the FEM of the monarch wing, the veins were modeled as rectangular, tapered, hollow structure, whereas the micro-CT scan suggests that the veins are circular, tapered, and hollowed (Fig. 1).

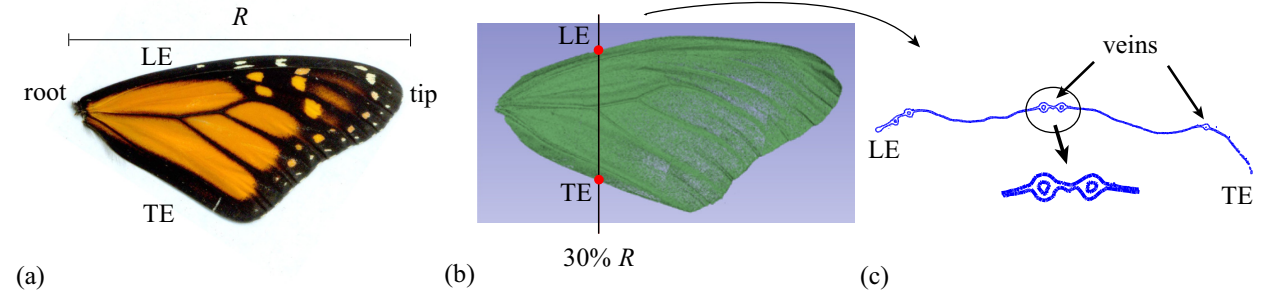


Fig. 1. (a) Monarch right forewing with a wing length of R (b) image of the micro-CT scan data of monarch butterfly forewing and (c) cross section of the wing at a spanwise location of 30 % R. Adapted from Twigg et al. [16].

In this work we report the effects of the vein structural model and, hence, the chordwise elastic modulus on the aerodynamic performance of monarch butterflies at different altitudes. We consider three representative vein models in this work: i) circular, tapered, solid; ii) circular, tapered, hollow and iii) circular, tapered, hollow, thin-walled veins. We calculate the chordwise elastic moduli for three vein models based on experimental data [32], where

deflection of real monarch wings are measured per given force. The FSI framework is the same as in our previous work [26]. We consider the plunge motion of a butterfly wing as a two-dimensional chordwise elastic flat plate and solve for the flow around the flexible wing. The three vein models are translated in the FSI model with the corresponding elastic modulus E of the wing. For each elastic modulus, the stroke plane angle E and air density E0 are varied. The changes in lift E1, thrust E2 and power E3 in each design space are calculated to characterize the effects of the elastic modulus on the monarch flight.

We summarize the key morphological and kinematic parameters relevant to monarch butterflies in Sections II.A and II.B. The three monarch vein structures and the corresponding elastic moduli are reported in Section II.C. The design space and non-dimensional parameters are described in Section II.D. The governing equations for fluid and structural dynamics are described in Sections II.E and the computational setup in Section II.F. Next, we discuss the aeroelastic response of the monarch scale wing with varying elastic modulus, altitude, and stroke plane angle in Section III. We provide concluding remarks in Section IV.

# II. Methodology

#### A. Morphological and Structural Parameters of Monarch Butterflies

Monarch butterflies have a pair of relatively large fore and hind wings which undergo large displacements and deformation during flight. The wings have veins embedded in them which run along spanwise and chordwise directions and give the wings directional stiffness. We define the fore wing length R as the distance between the wing root and the wing tip (Fig. 1). The total wing area S is defined as the area of all four wings in the overlapped configuration. The mean chord is calculated as  $c_m = S/(2R)$ . The non-dimensional radius to the second moment of wing area for the forewing is  $\hat{r}_2 = r_2/R$ , where  $r_2$  is the spanwise location of the second moment of wing area. In this study we consider the average morphological parameters from eight monarch specimens [26] as summarized in Table 1.

The structural parameters of the monarch butterfly forewing are determined from a representative butterfly specimen [16]. The thickness  $h_s$  of the forewing membrane along the chordwise direction at around 30 %R is  $54 \times 10^{-6}$  m. The wing density is  $\rho_s = 307$  kg/m<sup>3</sup>. The elastic modulus E of the wing in the chordwise direction is determined using a force-deflection experiment [16] with a linear FEM analysis (see Section II.C. and Appendix A).

Table 1. Monarch morphological parameters. From Sridhar et al. [26].

Parameter	Value
Total butterfly mass, <i>m</i> (kg)	$0.5 \times 10^{-3}$
Forewing length, $R$ (m)	$57 \times 10^{-3}$
Total wing area, $S(m^2)$	$34 \times 10^{-4}$
Non-dimensional radius to the second moment of wing area, $\hat{r}_2$	0.56
Mean chord, $c_{\rm m} = S/(2R)$ (m)	$30 \times 10^{-3}$

# **B.** Kinematic Parameters

We consider a two-dimensional plunge motion of a chordwise flexible wing as shown in Fig. 2. A sinusoidal plunge motion h with amplitude  $h_a$  and frequency f is imposed on the leading-edge (LE) of the wing as a function of time t. The non-dimensional form of the plunge motion can be written as

$$h^*(t^*) = St(\cos(2\pi t^*) - 1), \tag{1}$$

where  $t^* = tf$  is the non-dimensional time,  $St = 2fh_a/U$  is the Strouhal number and U is the freestream velocity representing the forward flight speed of the butterfly.

The kinematic parameters are based on 22 experimentally measured butterfly free flights in a pressure chamber recorded between simulated altitudes of 193 m and 4500 m [26]. The kinematic parameters are summarized in Table 2.

The thorax velocity magnitude is calculated by differentiating the thorax position in time and averaged over the length of each flight trajectory. The velocity magnitude varies between 0.77 m/s and 3.5 m/s with a mean velocity magnitude of 1.7 m/s. We consider a representative constant freestream velocity magnitude of U = 2 m/s in the current study.

The flapping angle  $\gamma$  is the angle between the left and the right forewings. The flapping frequency f is determined from the Fast Fourier Transform (FFT) of the time history of the flapping angle. The peak-to-peak flapping amplitude in a flapping cycle is calculated based on the time history of the angle between the forewings. The average flapping amplitude and flapping frequency are  $\gamma_{p2p} = 313$  deg and f = 10 Hz, respectively.

We calculate the plunge amplitude at the  $\hat{r}_2$  location based on the average peak-to-peak flapping amplitude  $\gamma_{p2p}$  and average wing length R as  $h_a = R\hat{r}_2\sin(\gamma_{p2p}/4)$ . The plunge amplitude varies between  $h_a = 30$  mm and  $h_a = 32$  mm with an average of  $h_a = 31$  mm. We consider a plunge amplitude of  $h_a = 31$  mm in the current study.

The stroke plane angle  $\beta$  is the angle between the longitudinal body axis and the normal to the plane containing the wing tip positions during flight. The measured stroke plane angle varied between  $\beta = 3.3$  deg and  $\beta = 33$  deg. The stroke plane angle is left as a design variable in this study.

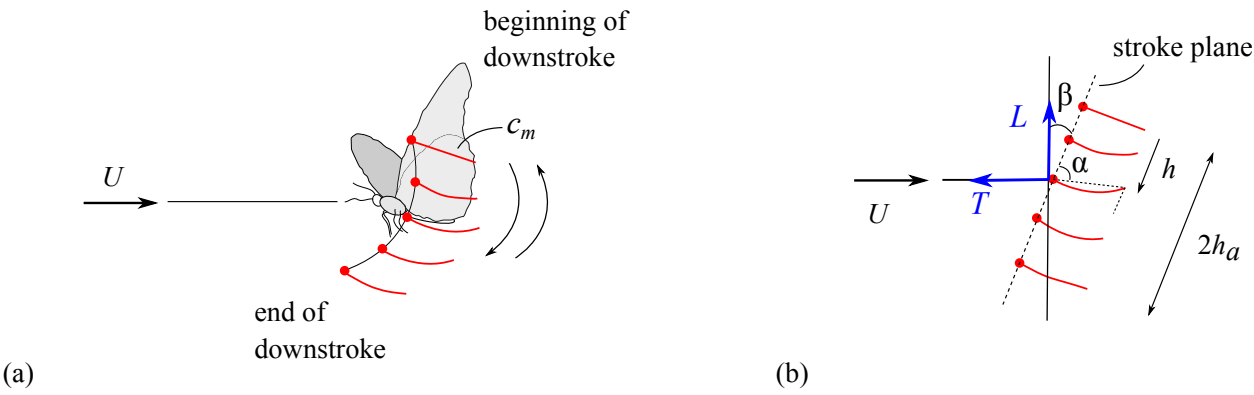


Fig. 2. (a) Schematic showing the flapping wing motion and the (b) corresponding plunge motion with an amplitude of  $h_a$ . Lift and thrust directions are indicated relative to the freestream direction. Passive pitch angle is denoted by  $\alpha$ . Red dots indicate the LE. From Sridhar et al. [26].

Table 2. Kinematic parameters determined from experimental free flight measurements.

Kinematic variable	Value	Experimental Observation
Freestream velocity, $U(m/s)$	1.7	0.77 - 3.5
Flapping frequency, $f(Hz)$	10	10
Peak-to-peak flapping amplitude, $\gamma_{p2p}$ (deg)	313	313
Plunge amplitude, $h_a$ (mm)	31	30 - 32
Stroke plane angle, β (deg)	17	3.3 - 33

#### C. Elastic Modulus of the Wing

Monarch wings are anisotropic with hollow veins [16]. As depicted in Fig. 1, the monarch veins are circular shaped, tapered from the root toward the tip, and hollow. Because the detailed vein structure affects the stiffness of the wing, we create three monarch wing models from a high resolution micro-CT scanned image of a monarch wing [16]. Here, we consider three vein structural models: i) circular, tapered, solid; ii) circular, tapered, hollow (baseline: closest to the real wing); and iii) circular, tapered hollow with thin-walled veins (Fig. 3). The thinner vein wing model in Fig. 3c is created based on half the thickness of the veins of the circular, tapered, hollow model in Fig. 3b.

We determine the corresponding elastic modulus for each of the wing models based on a series of force-deflection experiment on a set of real monarch wings [16,32]. In our previous work [26], we modeled the veins as rectangular, tapered, hollow structures, which yield a chordwise elastic modulus of 0.2 GPa. In this study, we repeated the process for the three vein structures. The resulting elastic moduli for the three vein structures are shown in Table 3. The elastic modulus is the lowest for the solid veins, followed by the baseline model. The elastic modulus is the highest for the veins with the thinner walls.

Based on the elastic modulus determined from the FEM analysis (Table 3), we select four representative chordwise elastic moduli to investigate the aeroelastic effects of the vein structures on the FSI of monarch wings: E = 0.2, 0.3, 0.4 and 0.8 GPa.

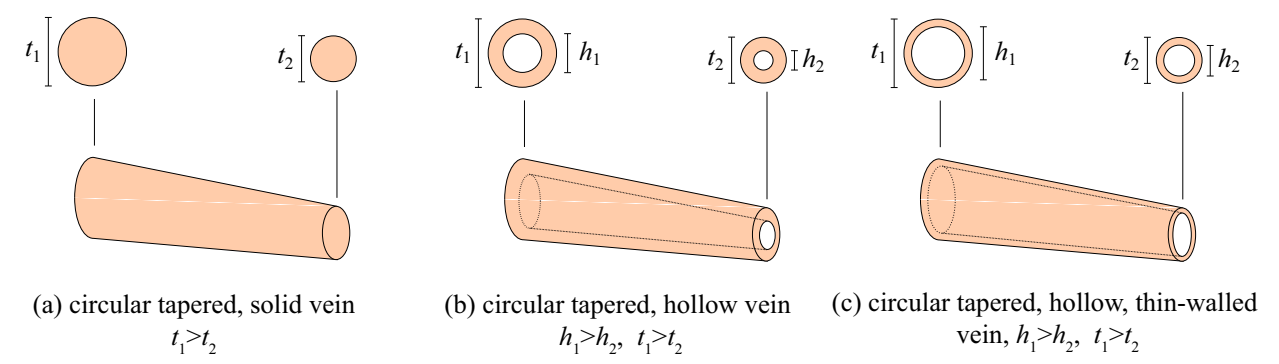


Fig. 3. Schematic of the vein structural models. (a) Circular, tapered, solid vein (b) baseline wing model with circular, tapered, hollow vein which closely resembles real monarch wing, (c) circular, tapered, hollow, thinwalled vein model.

Table 3. Chordwise elastic moduli calculated from linear FEM analysis for three vein models. See Appendix A for detailed results of the FEM analysis.

Vein Structure Model	Chordwise Elastic Modulus, E (GPa)	Spanwise Elastic Modulus, (GPa)
Circular, tapered, solid (Fig. 3a)	0.22	2.4
Circular, tapered, hollow (Fig. 3b): baseline	0.3	2.5
Circular, tapered, hollow with thin-walled veins (Fig. 3c)	0.33	3.2

#### D. Design Space and Non-dimensional Parameters

Figure 4a shows the variation of air density with increase in altitude [15]. Monarchs encounter varying altitudes during their long-range migration. In addition to flying at sea level conditions, monarch butterflies fly at higher altitudes [4] and have been spotted at around 1200 m above sea level. Furthermore, the overwintering mountains in Central Mexico where Monarchs gather in millions are located at altitudes between 2900 m and 3200 m [9–13].

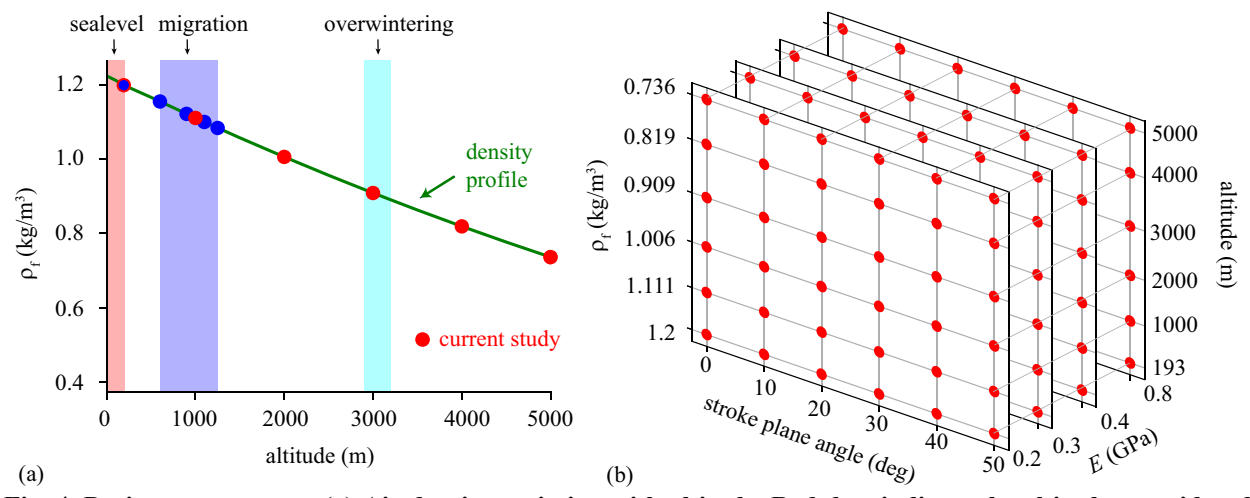


Fig. 4. Design space set up. (a) Air density variation with altitude. Red dots indicate the altitudes considered in the current study. The flight altitudes at which monarchs were spotted [4] are shown as blue dots. (b) Three-dimensional design space with design variables air density  $\rho_f$ , stroke plane angle  $\beta$ , and elastic modulus E.

In this study, we consider four design spaces (Fig. 4b) for each of the four elastic moduli (E = 0.2, 0.3, 0.4 and 0.8 GPa) with the air density  $\rho_f$  and the stroke plane angle  $\beta$  as the design variables to assess the effects of altitude on the aerodynamic performance at monarch butterfly scale. Six altitudes are considered between 193 m and

5000 m. The corresponding air density at these altitudes varies between  $\rho_f = 1.2 \text{ kg/m}^3$  and  $\rho_f = 0.736 \text{ kg/m}^3$ . We consider six stroke plane angles between  $\beta = 0$  deg and  $\beta = 50$  deg with 10 deg increments. The resulting design space consists of 144 design points. Other parameters are kept constant in this study.

We characterize the flapping wing aerodynamics in forward flight by four non-dimensional variables [33]: Reynolds number Re, Strouhal number St, reduced frequency  $k = \pi f c_m/U$ , and stroke plane angle  $\beta$ . The Reynolds number describes the relative importance of fluid inertia and viscous effects. The Strouhal number compares the velocity of the wing tip to the forward flight of the butterfly. The reduced frequency characterizes the unsteadiness in the flow field. In the considered altitude range between 193 m and 5000 m (Fig. 4), the Reynolds number varies between Re = 3913 and Re = 2400 due to the change in air density. The Strouhal number remains constant at St = 0.36 and the reduced frequency was also constant at k = 0.47 in this study.

Additional dimensionless parameters arise when a flexible wing is considered [22]. The three non-dimensional structural parameters are the density ratio  $\rho^*$ , thickness ratio  $h_s^*$ , and the frequency ratio  $f/f_1$ . The density of air varies between 1.2 kg/m³ and 0.736 kg/m³ between the considered altitude range of 193 m and 5000 m [15]. The density of monarch wings is 307 kg/m³ [16]. The density ratio  $\rho^* = \rho_s/\rho_f$ , where  $\rho_s$  is the wing density, varies between  $\rho^* = 256$  and  $\rho^* = 417$ . The thickness ratio  $h_s^* = h_s/c_m$  is the wing thickness normalized by the mean chord. The thickness ratio calculated based on wing membrane thickness is  $h_s^* = 1.8 \times 10^{-3}$  (Table 4). Finally, the frequency ratio is  $f/f_1 = 2\pi f c_m \sqrt{12\rho_w/E} / (k_1^2 h_s^*)$  defined as the ratio of the flapping frequency f and the first natural frequency of the wing in chordwise direction  $f_1$  [22,31], where  $k_1 = 1.875$ . The frequency ratio varied inversely as the chordwise elastic modulus of the wing E. The non-dimensional parameters are summarized in Table 4.

Table 4. Non-dimensional variables at the monarch butterflies scale considered in the current study. Adapted from Sridhar et al. [26].

Non-dimensional variable	Value
Reynolds number, $Re = \rho_f U c_m / \mu$	3913 - 2400
Reduced frequency, $k = \pi f c_m / U$	0.47
Strouhal number, $St = 2fh_a/U$	0.31
Thickness ratio, $h_s^* = h_s/c_m$	$1.8 \times 10^{-3}$
Density ratio, $\rho^* = \rho_s/\rho_f$	256 - 417
	1.22 (circular, tapered, solid vein)
Frequency ratio, $f/f_1$	1.04 (circular, tapered, hollow vein): baseline
	0.99 (circular, tapered, hollow, thin-walled vein)
Stroke plane angle, β (deg)	0 - 50

#### E. Governing Equations

A constant density  $\rho_f$  and viscosity  $\mu$  flow field is governed by the unsteady Navier-Stokes equations expressed by,

$$\nabla^* \cdot \mathbf{u}^* = 0$$

$$\frac{k}{\pi} \frac{\partial \mathbf{u}^*}{\partial t^*} + (\mathbf{u}^* \cdot \nabla^*) \mathbf{u}^* = -\nabla^* p^* + \frac{1}{Re} \Delta^* \mathbf{u}^*$$
(2)

with the velocity  $\mathbf{u}$ , pressure p, and time t. The superscript (\*) indicates dimensionless variables. The dimensional variables are non-dimensionalized with a freestream velocity U, inverse of the motion frequency 1/f, and chord c, respectively.

We consider a two-dimensional, elastic wing structure with uniform thickness  $h_s$ , density  $\rho_s$ , and elastic modulus E. As the flat plate follows the imposed vertical motion described by Eq. (1) at the LE, the resulting fluid dynamic force dynamically balances with the wing inertia and the elastic bending forces. This was modeled locally as a linear Euler-Bernoulli beam [17] as

$$\frac{\partial^2 w^*}{\partial t^{*2}} + \frac{4\pi^2}{k_1^4} \left(\frac{f_1}{f}\right)^2 \frac{\partial^4 w^*}{\partial x^{*4}} = \frac{p^*}{h_s^* \rho^*} \left(\frac{\pi}{k}\right)^2, \tag{3}$$

where  $w^* = w/c$  is the displacement due to bending motion,  $f/f_1$  is the frequency ratio, and  $k_1 = 1.875$  is the first root corresponding to first natural frequency of the wing.

The resulting wing camber deformations  $(w-h)/c_m$  can also be regarded as a pitch rotation  $\alpha(t^*)$ , the angle between the trailing-edge (TE) and the leading-edge (LE), see Fig. 2b. Passive pitch angle acts as an effective angle of attack, measured in terms of the angular amplitude  $\alpha_a$  and the phase lag  $\phi$ . To characterize the pitch angle, we use the passive pitch angular amplitude  $\alpha_a$  and phase lag  $\phi$  by approximating the pitch by a first-order harmonic as

$$\alpha_{\rm FH} = 90^{\circ} - \alpha_{\rm a} \cos(2\pi t^* + \phi). \tag{4}$$

The wing deformation relative to the imposed plunge motion h at the LE is calculated by v = w-h. We determine the wing deformations at the TE of the wing at the middle  $v_m = v^*(0.25)$  and the end of the strokes  $v_e = v^*(0.5)$ . The relative wing deformations are then converted to passive pitch angle as  $\alpha_m = \arctan(v_m)$  and  $\alpha_e = \arctan(v_e)$ . Based on these two angles, a first-order harmonic approximation can be constructed for the passive pitch of Eq. (4), by solving for the phase lag  $\phi$  and the angular amplitude  $\alpha_a$  with  $\alpha_{EH}(0.25) = \alpha_m$  and  $\alpha_{EH}(0.5) = \alpha_e$ .

The effective angle of attack is a key aerodynamic parameter and was defined based on the instantaneous plunge motion and the passive pitch as

$$\alpha_{\text{eff}}(t) = -\arctan\left(\frac{w(t) - h(t)}{c_m}\right) - \arctan\left(\frac{\dot{h}(t)}{U}\right) + \beta.$$
 (5)

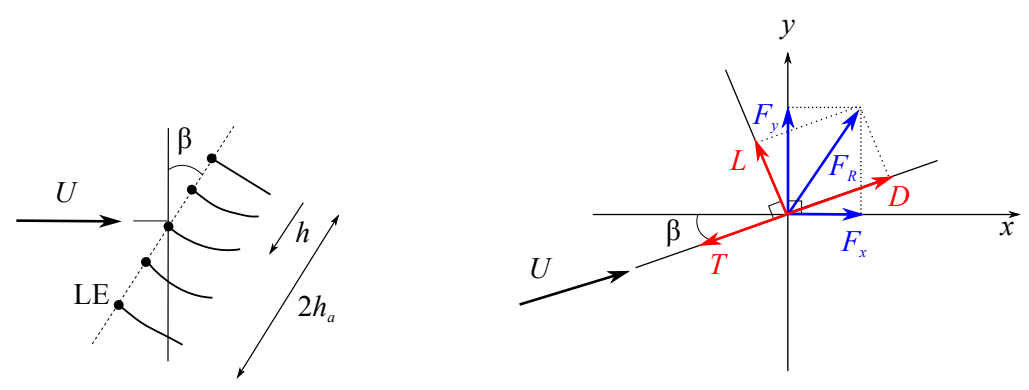


Fig. 5. Plunge motion and definitions of lift and thrust relative to the freestream U and stroke plane angle  $\beta$ .

The aerodynamic performance is evaluated using three quantities: lift, thrust and power. The lift and thrust are calculated using the horizontal and vertical force components at a given stroke plane angle  $\beta$  (Fig. 5) as

$$L(t) = 2R \left( F_{y}(t) \cos \beta - F_{x}(t) \sin \beta \right)$$
  

$$T(t) = -2R \left( F_{y}(t) \sin \beta + F_{x}(t) \cos \beta \right),$$
(6)

where  $F_x$  and  $F_y$  are the horizontal and vertical components of force per unit span, respectively, L and T are the lift and thrust (Fig. 5) which are perpendicular and parallel to the freestream direction, respectively.

When calculating the cycle averaged quantities, denoted by ( ), we avoid the initial transients by carrying out the time averaging over the third motion cycle. The time-averaged lift for example is defined as

$$\overline{L} = \frac{1}{T} \int_{T}^{2T} L(t)dt. \tag{7}$$

The time-averaged lift coefficient, excess lift coefficient, and thrust coefficient are defined as

$$\bar{C}_{L} = \frac{\bar{L}}{0.5\rho_{f}U^{2}(2R)c_{m}}, \qquad \bar{C}_{L,excess} = \frac{\bar{L} - W_{b}}{0.5\rho_{f}U^{2}(2R)c_{m}}, \qquad \bar{C}_{T} = \frac{\bar{T}}{0.5\rho_{f}U^{2}(2R)c_{m}},$$
(8)

where  $W_b = mg$  is the butterfly weight.

To measure the cost of performance, we define the time-averaged power as

$$\overline{P} = \frac{-2R}{T} \int_{T}^{2T} F_{y}(t) \dot{h}(t) dt - \frac{2R}{T} \int_{T}^{2T} \dot{h}(t) \int_{LF}^{TE} \rho_{s} h_{s} \ddot{w}(t) dx dt.$$
(9)

The second term in the above equation represents the inertial power associated with the wing motion.

# F. Numerical Models and Computational Setup

The aerodynamic forces and moments are calculated directly by the coupled Navier–Stokes equations (Eq. (2)) and structural dynamics solvers (Eq. (3)) under the imposed kinematics (Eq. (1)), by integrating the pressure and shear forces on the wing. We use an in-house, structured, pressure-based finite volume solver to solve for Eq. (2) that governs the motion of the fluid [22,27,28,31]. The convection terms are discretized using a second-order upwind scheme, and the pressure and viscous terms are treated with second-order central difference schemes. An implicit Euler scheme is used for time integration.

We solve Eq. (3) using a finite element representation of the Euler–Bernoulli beam model. The wing is modeled by a flat plate with 51 equally distributed nodes. The two degrees of freedom included in the model are the transverse displacement and bending. For qualitative investigation of the flexible flapping wing aeroelasticity, a linear Euler–Bernoulli beam model is sufficient for a chordwise flexible airfoil [22]. Radial basis function interpolation is used to deform the mesh [34].

The governing Eqs. (2) and (3) for the fluid and structure, respectively, are solved independently. The fluid-structure interaction coupling is a time-domain partitioned process. At each time step the fluid and structural solutions are iterated until sufficient convergence is reached for the displacement of the flexible wing within an inner-iteration before advancing to the next time step. Details of the fluid-structure interaction and careful validation studies against well-documented experimental results are shown in our previous work [22,27,28].

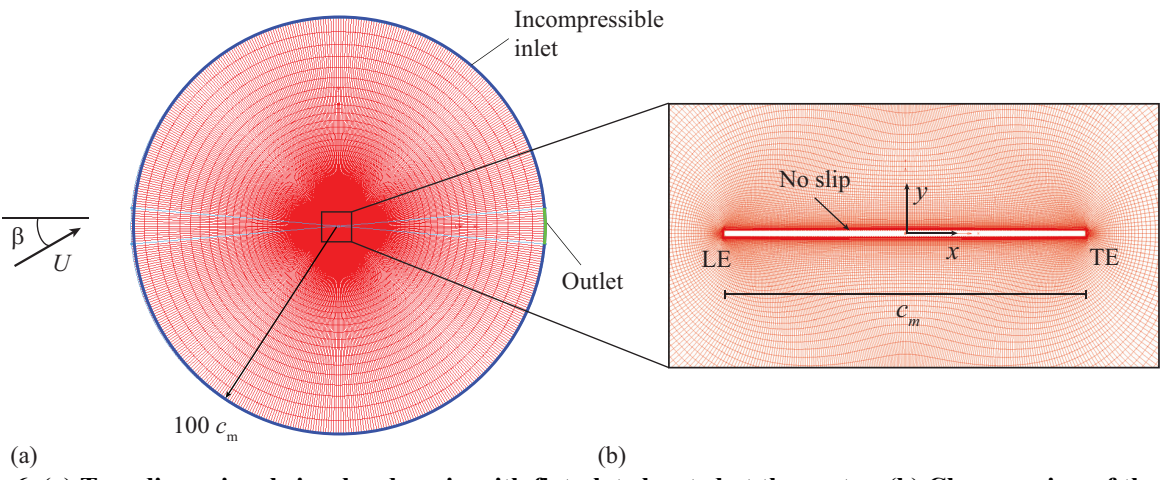


Fig. 6. (a) Two-dimensional circular domain with flat plate located at the center. (b) Close up view of the grid around the flat plate. Incompressible inlet boundary condition is prescribed at the inlet with freestream velocity U = 2 m/s and no-slip boundary condition on the flat plate. The outer boundary is located at a radius of  $100c_{\rm m}$  from the domain center. From Sridhar et al. [26].

The computational domain is shown in Fig. 6a with a  $0.02c_{\rm m}$  thick flat plate at the center of the domain with the outer boundary located at a radial distance of  $100c_{\rm m}$ . We impose a freestream velocity U at the inlet of the computational domain as shown in Fig. 6a. A no-slip condition is imposed on the flat plate surface. A fixed zero-pressure condition is set at the outlet boundary. The time step and grid sensitivity results can be found in the Appendix B and the details of the computational setup are discussed in our previous work [26].

#### III. Results and Discussion

# A. Lift, Thrust and Power Variation

The variation of mean aerodynamic variables with the altitude and stroke plane angle is shown in Fig. 7 for the three elastic moduli. All motions in the design space generate positive mean lift at all altitudes. At lower stroke plane angles, the mean lift is close to zero. As the stroke plane increases, the mean lift increases. The equilibrium lift  $\bar{L} = W_b = 4.9$  mN to maintain the butterfly weight is indicated by a black line in Fig. 7a-c.

For the softest wing with E=0.2 GPa, which corresponds to a vein structure with a thinner wall, the equilibrium lift is generated when the stroke plane angle is  $\beta=32$  deg at the altitude of 193 m and  $\beta=35$  deg at 3000 m. For the stiffest wing, the lift is higher in general and the variation of lift is more sensitive to the stroke plane angle than the air density. The relatively insensitive nature of the lift with respect to air density suggests that the role of the FSI is weaker for this stiffer wing. For the baseline wing (E=0.3 GPa), the equilibrium lift is found when  $\beta=31.3$  deg at 3000 m (Fig. 7), which is within the experimentally observed stroke plane angle range of  $\beta=[3,33]$  deg.

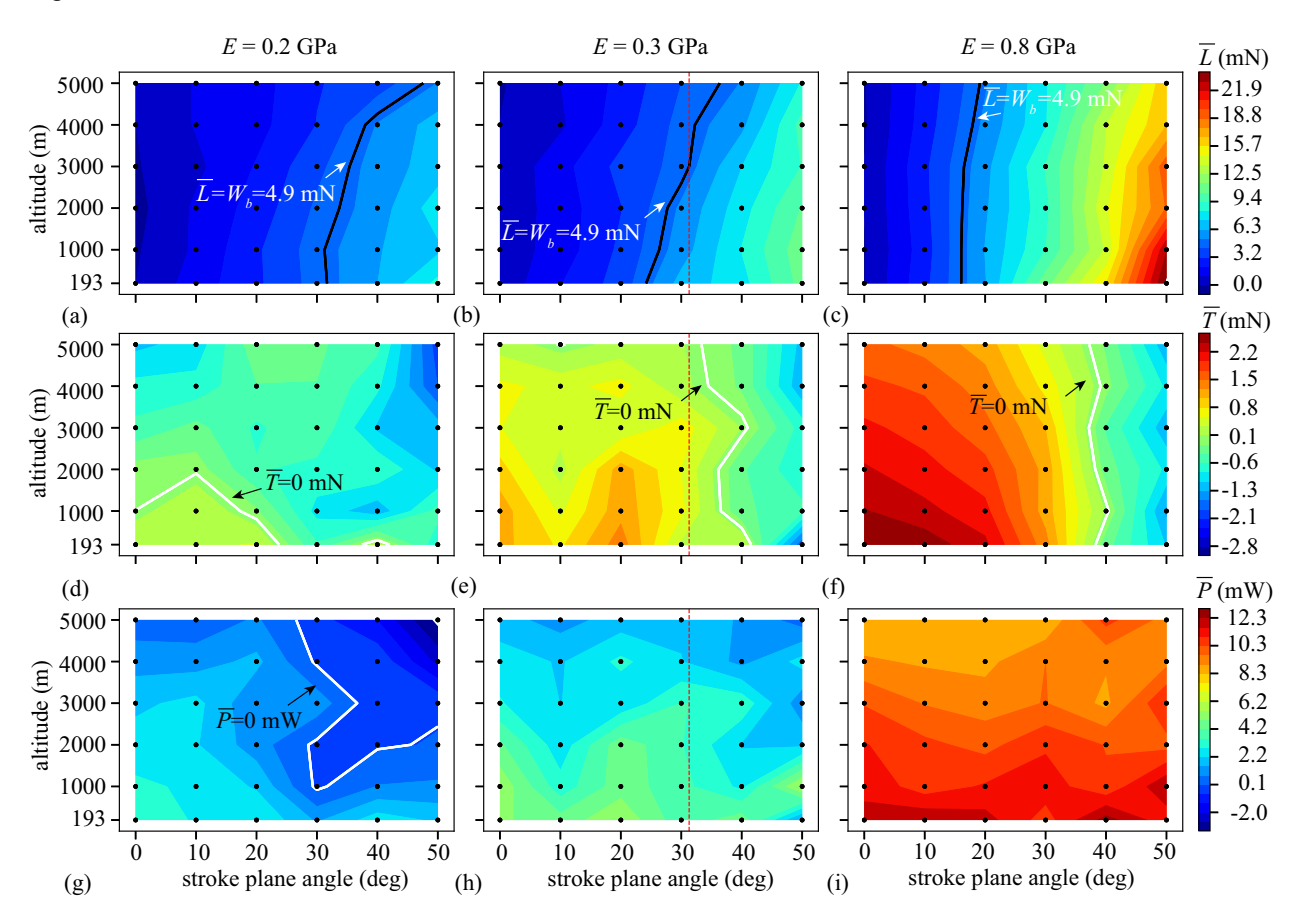


Fig. 7. Contours of mean (a-c) lift, (d-f) thrust and (g-i) power with respect to changes in altitude and stroke plane angle for E = 0.2, 0.3, and 0.8 GPa. The design points are shown as black dots. Black line in (a-c) indicates the equilibrium butterfly weight  $W_b = 4.9$  mN. The white lines in (d-g) indicate the zero thrust and power contour level. The vertical dotted line in (b,e,h) indicates the stroke plane angle corresponding to equilibrium lift at 3000 m and E = 0.3 GPa.

The mean thrust (Fig. 7d-f) is in general lower compared to the mean lift. As seen with lift, the magnitude of mean thrust increases with elastic modulus. The thrust decreases with the stroke plane angle and the altitude. Eventually the thrust becomes negative, i.e. the resulting aerodynamic force is pointed in the streamwise direction, contributing to the drag. The region in the design space, where the thrust begins contributing to the drag ( $\overline{T} = 0$ ), is indicated by the white line. At E = 0.2 GPa, the thrust is generally negative (i.e. drag), except when the stroke plane

angle and the altitude are both low. At E = 0.3 and 0.8 GPa, the negative thrust is confined to higher stroke plane angles. At the overwintering altitude of 3000 m, the thrust is small but still positive, implying that the monarchs mostly fly with a constant speed, whereas at sea-level conditions the monarchs can generate large propulsive forces for rapid accelerations.

The power required (Fig. 7g-i) is lower with softer wings and increases as the wing stiffness increases. Furthermore, at higher altitude the power required is lower than at the sea-level for the three elastic moduli. At E = 0.2 GPa, higher stroke plane angle and higher altitude yields negative power denoted by the white line.

# B. Angular Amplitude, Phase Lag and Effective Angle of Attack at $\beta = 31.3$ deg

The passive pitch angle, defined as the angle between the trailing edge and the leading edge due to the deformation of the flexible chordwise wing, is measured in terms of the passive pitch amplitude  $\alpha_a$  and phase lag  $\phi$  (Section II.E.). The passive pitch amplitude measures the magnitude of the wing deflection. For the softest wing, (E=0.2 GPa),  $\alpha_a$  is relatively more sensitive to the air density varying between 48 and 56 deg. As the wing stiffens, at 3000 m, the passive pitch decreases from 55 deg at E=0.3 GPa to 49 deg at E=0.8 Gpa.

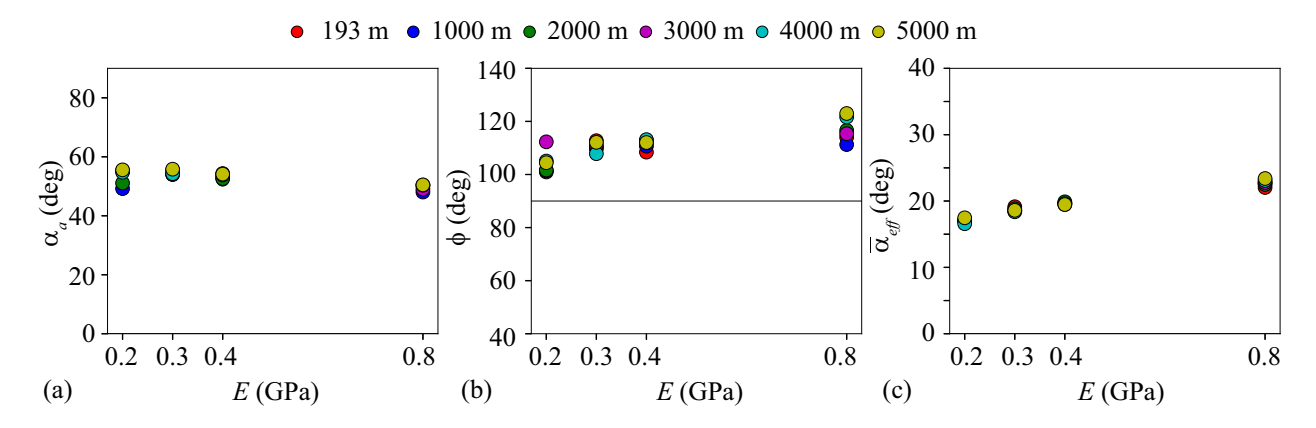


Fig. 8. Mean (a) passive pitch amplitude, (b) phase offset, and (c) effective angle of attack with respect to changes in elastic modulus E at stroke plane angle of  $\beta = 31.3$  deg.

The phase lag  $\phi$  represents the lag of the TE motion relative to the LE. At E = 0.2 GPa, the phase lag at stroke plane of 31.3 deg varied between 101 deg and 112 deg, implying that the TE lags the LE.

The effective angle of attack  $\alpha_{\rm eff}$  is a key aerodynamic parameter, which is defined as the combined outcome of the angle due to the instantaneous plunge motion, passive pitch and the stroke plane angle. Figure 8c shows that the effective angle is insensitive to the air density. In general,  $\alpha_{\rm eff}$  increases with the stiffness. For example, at 3000 m, the effective angle of attack increases from 17 deg at E=0.2 GPa to 23 deg at E=0.8 GPa.

#### C. Lift, Thrust and Power Coefficients

The excess mean lift, thrust and power coefficients are shown in Fig. 9 with respect to the elastic modulus at the stroke plane angle of  $\beta = 31.3$  deg. The excess mean lift is the coefficient of the excess lift relative to the weight (Eq. (8)). This lift coefficient increases with the elastic modulus with the highest  $\overline{C}_{L,excess} = 0.83$  and  $\overline{C}_L = 1.62$  at E = 0.8 GPa and 3000 m. The mean thrust is close to zero and slightly increases with the elastic modulus. That said,  $\overline{C}_T < 0$  at E = 0.2 GPa for all altitudes, implying that the wings modeled with solid veins cannot generate thrust to accelerate. Finally, the power coefficient is lower for softer wings and power coefficient increases with increasing elastic modulus. Therefore, both the excess lift and thrust coefficients are larger in general as the wing stiffens but the required power consumption is also the highest.

The lift coefficient depends strongly on the effective angle of attack  $\alpha_{\rm eff}$  (Fig. 10). The relation between  $\overline{C}_{\rm L}$  and  $\alpha_{\rm eff}$  is nearly linear. The lift curve slope increases as the wing stiffness increases with  $d\overline{C}_{\rm L}/d\alpha_{\rm eff}=5.2~{\rm rad}^{-1}$  at  $E=0.3~{\rm GPa}$  and 10.8 rad<sup>-1</sup> at  $E=0.8~{\rm GPa}$ . The lift curve slope at  $E=0.8~{\rm GPa}$  is higher than the classical thin airfoil theory slope of  $2\pi$ . The slopes for E=0.2 and 0.3 GPa are lower than the classical solution. These results indicate that the wing flexibility strongly affects the resulting lift generation without the need of an active controller.

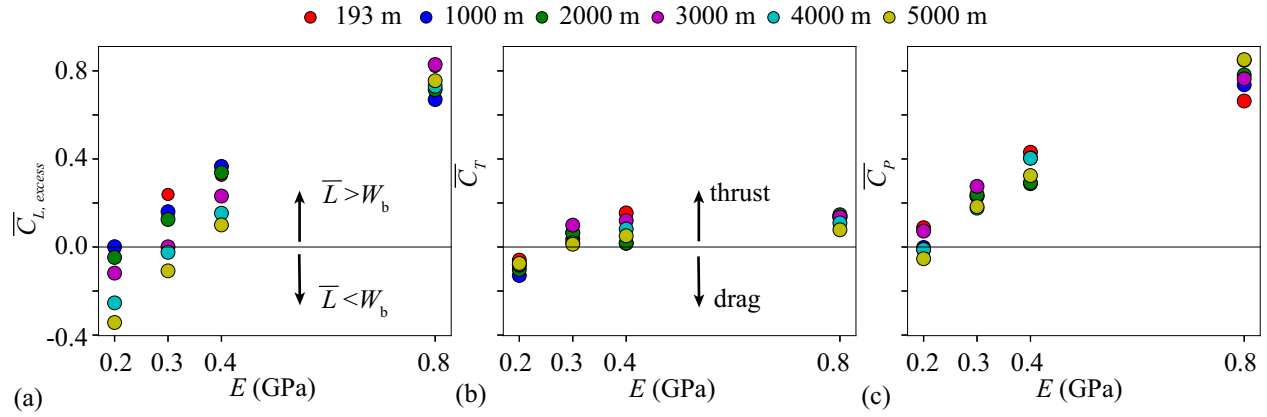


Fig. 9. Mean (a) excess lift coefficient, (b) thrust coefficient, and (c) power coefficient with elastic modulus E at stroke plane angle of  $\beta = 31.3$  deg.

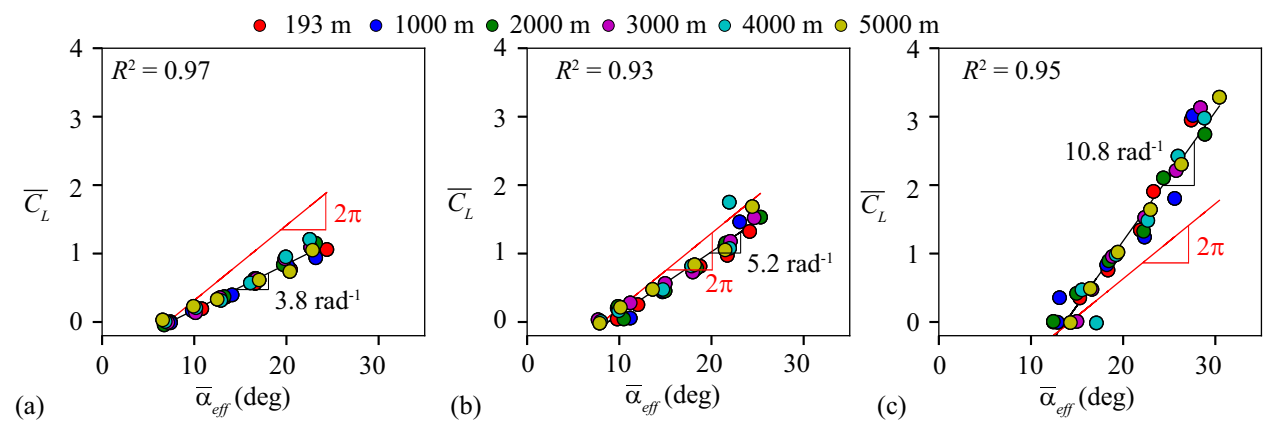


Fig. 10. Variation of mean lift coefficient with effective angle of attack at (a) E = 0.2 GPa, (b) E = 0.3 GPa, and (c) E = 0.8 GPa.

# **IV.** Concluding Remarks

The physical understanding of the aerodynamic mechanisms behind long range migration of monarch butterflies is currently underexplored. Monarch butterflies have large pairs of anisotropic wings which undergo significant deformation during flight. Furthermore, they migrate at altitudes as high as 1200 m and all the overwintering sites are located at altitudes near 3000 m, where the air density is significantly lower than at the sea-level.

In this study, we report the effects of different vein structural model and the corresponding elastic modulus of a monarch scale wing on the aerodynamic performance. We use a well-validated fully-coupled Navier-Stokes solver with a structural dynamics solver. Chordwise cross-section of a monarch scale wing is considered under a constant freestream flow, representing a forward flight. The altitude effects are simulated by adjusting the air density. The stroke plane angle, the elastic modulus of the wing, and air density are changed.

Our results show that the propulsive force generation and the power consumption significantly depend on the elastic modulus and hence, the vein structural model. The lift and thrust in general increase with the stiffness and stroke plane angle. Furthermore, the force magnitudes decrease with the altitude. The mean power required reduces with the stiffness, implying that softer wings required less power than stiffer wings at a given stroke plane angle and altitude.

The elastic modulus of the vein structural model that corresponds the closest to the micro-CT scanned image of a monarch wing is E = 0.3 GPa. When E = 0.3 GPa, sufficient lift can be generated by adjusting the stroke plane angle in a range that is observed from freely flying monarchs. Furthermore, at the sea-level the thrust is relatively large as well as the power consumption. On the other hand, at the overwintering altitude, the thrust is much smaller yet positive and the power consumption is also much lower.

We propose the existence of two monarch flight modes based on the results: i) at the sea-level, the stroke plane angle  $\beta$  can be as small as 24 deg to generate sufficient lift to fly. The thrust is nearly as large as the lift, which can be used to climb or perform rapid maneuvers; ii) at the migration/overwintering altitude, the lift is smaller, just enough to stay aloft at  $\beta = 31$  deg. Furthermore, the thrust is still positive but much smaller. This suggests that the monarchs cannot rapidly accelerate as seen at the sea-level. That said, the power consumption at  $\beta = 31.3$  deg and 3000 m is about 10 % lower compared to that at 193 m. Faced with difficulties of food intake during migration and overwintering, the monarchs may be operating in an energy efficient mode by utilizing their flexible wing structures.

Finally, these results suggest that bioinspired micro flying robots can benefit from using flexible wing structures. Not only is the power consumption much lower with a more flexible wing, by changing the wing stiffness or the flight altitude, the resulting force generation and power consumption can be modulated. A better understanding of this fluid-structure interaction can help designing next-generation highly efficient long-range drones.

# Acknowledgments

We thank Rachel Twigg, Clifford Tatum and Jared Sampson for their assistance with the monarch butterfly measurements. This work is supported by NSF CMMI-1761618.

# **Appendix**

#### A. Determination of Elastic Modulus for the Monarch Vein Models from FEM

The experimentally measured mean forces and their corresponding deflections [32] in the chordwise and spanwise directions for monarch wings are shown Fig. A1. A linear fit of the force and deflection is constructed by accounting for the zero deflection at the no-load condition (red data point in Fig. A1). The intercept of this linear fit is set to zero. Based on the obtained linear fit between the applied force and the deflection, we choose six intermediate points as input to the FEM modeling of the three vein structures in Fig. 3. These are indicated by  $F_{\text{lin}}$  and  $\delta_{\text{lin}}$  in Tables A1 and A2.

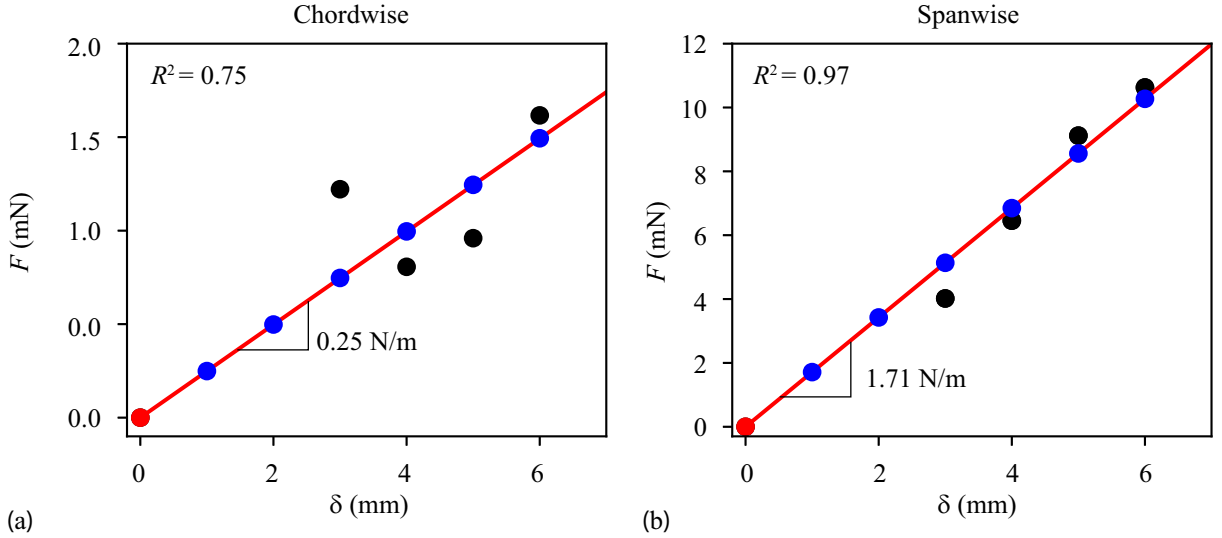


Fig. A1. Forces and corresponding deflection in (a) chordwise and (b) spanwise directions. Black dots indicate the experimentally measured data [16]. Blue dots indicate the data points chosen for the FEM analysis corresponding to  $F_{\rm lin}$  and  $\delta_{\rm lin}$  in Tables A1 and A2.

Using the methodology described in Section II.C. and by Twigg et al. [16], we determine the chordwise elastic modulus for the three vein structures in Fig. 3. The elastic modulus for the three wing models is determined such that the deflection from the FEM  $\delta_{\text{FEM}}$  matched the reference deflection  $\delta_{\text{lin}}$  for a given  $F_{\text{lin}}$ . The resulting elastic modulus and the percentage error in the deflection  $\delta_{\text{error}} = (\delta_{\text{lin}} - \delta_{\text{FEM}})/\delta_{\text{FEM}}$  are shown in Tables A1 and A2.

Table A1. Elastic modulus in the chordwise direction for three vein structures determined using the FEM analysis.

		Circular, tapered, solid			Circular, tapered, hollow			Circular, tapered, hollow, thin-		
			veins		veins			walled veins		
$F_{lin}$ (mN)	$\begin{array}{c} \delta_{lin} \\ (mm) \end{array}$	E <sub>FEM</sub> (GPa)	$\delta_{\text{FEM}} \ (\text{mm})$	$\delta_{ m error} \ (\%)$	E <sub>FEM</sub> (GPa)	$\delta_{\text{FEM}}$ (mm)	$\delta_{\text{error}} $ (%)	$E_{\rm FEM}$ (GPa)	$\delta_{\text{FEM}}$ (mm)	$\delta_{ m error} \ (\%)$
0.25	1		0.98	-1.8		1.01	1		0.99	-0.3
0.5	2		1.97	-1.5		2.01	0.5		1.99	-0.5
0.75	3	0.22	2.95	-1.7	0.2	3.02	0.7	0.22	2.99	-0.3
1.00	4	0.22	3.93	-1.7	0.3	4.02	0.5	0.33	3.98	-0.5
1.25	5		4.91	-1.8		5.03	0.6		4.98	-0.4
1.5	6		5.85	-2.5		5.99	-0.2		5.98	-0.3

Table A2. Elastic modulus in the spanwise direction for three vein structures determined using the FEM analysis.

		Circular, tapered, solid			Circular, tapered, hollow			Circular, tapered, hollow, thin-		
			veins		veins			walled veins		
F <sub>lin</sub> (mN)	$\delta_{lin}$ (mm)	E <sub>FEM</sub> (GPa)	$\delta_{\text{FEM}}$ (mm)	$\delta_{ m error} \ (\%)$	E <sub>FEM</sub> (GPa)	$\delta_{\text{FEM}}$ (mm)	$\delta_{\text{error}}$ (%)	E <sub>FEM</sub> (GPa)	$\delta_{\text{FEM}}$ (mm)	δ <sub>error</sub> (%)
1.71	1		1.02	2		1.02	2		0.99	-0.8
3.42	2		2.04	2		2.03	1.5		1.98	-1
5.14	3	2.4	3.07	2.33	2.5	3.06	2	2.2	2.98	-0.67
6.85	4	2.4	4.09	2.25	2.5	4.1	2.5	3.2	3.97	-0.75
8.56	5		5.1	2		5.09	1.8		4.96	-0.8
10.27	6		6.13	2.17		6.11	1.83		5.96	-0.67

# B. Grid and Timestep Sensitivity Study

Grid and timestep sensitivity studies are performed with a rigid wing at Re = 5869, k = 0.31, and St = 0.21 at a stroke plane angle of  $\beta = 0$  deg. We use a representative pitch and plunge motion to assess the grid and time step sensitivity with a sinusoidal pitch amplitude of 30 deg and a phase lag of 90 deg. The pitch axis is located at the center of the flat plate. The plunge amplitude is 31 mm. Five levels of grids are considered with 31 to 481 points on the wing (Table B1). A freestream velocity of U = 3 m/s is prescribed at the domain inlet (Fig. 6a). For each grid level, we calculate the  $L_1$ ,  $L_2$  and  $L_\infty$  norm of lift and thrust coefficients for two flapping cycles between  $t^* = 2$  and  $t^* = 3$  with the solution at finest grid (481 points) considered as the most accurate solution.

Time variation of lift and thrust coefficient is shown for three flapping cycles in Fig. B1 for the five grid levels. All three norms show convergence. Based on Fig. B1 and Table B1, the grid with 241 points on the wing is chosen as the optimal grid for all computations.

Table B1. Grid sensitivity results for two-dimensional rigid wing motion. The norms for  $C_L$  and  $C_T$  are calculated between  $t^* = 2$  and  $t^* = 3$ .

Grid		$C_{ m L}$		$C_{\mathrm{T}}$			
		$L_1$ norm	$L_2$ norm	$L_{\infty}$ norm	$L_1$ norm	$L_2$ norm	$L_{\infty}$ norm
31	5,950	149.809	5.173	0.228	61.865	2.375	0.131
61	13,736	109.886	3.862	0.181	44.973	1.771	0.104
121	31,388	66.998	2.318	0.127	25.362	0.981	0.062
241(baseline)	70,104	22.271	0.895	0.064	5.236	0.198	0.016
481	156,058	-	-	-	-	-	-

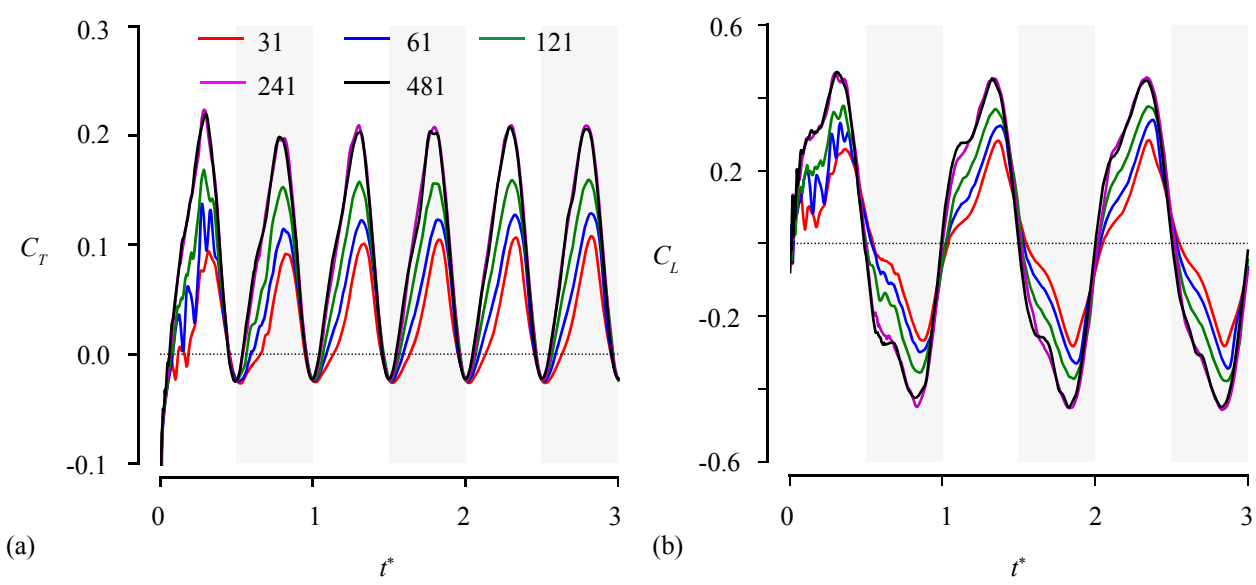


Fig. B1. Grid convergence study with five different grid levels. Time history of (a) thrust and (b) lift coefficients for three flapping cycles.

Timestep sensitivity is performed with the converged grid with 241 points on the wing. We consider six timestep levels as shown in Table B2. For each timestep, we calculate the lift and thrust coefficients as shown in Fig. B2. Again, all the norms showed convergence. The timestep of  $\Delta t = 1.041 \times 10^{-4}$  s is chosen as the converged timestep for all computations. This corresponds to 960 timesteps per flapping cycle.

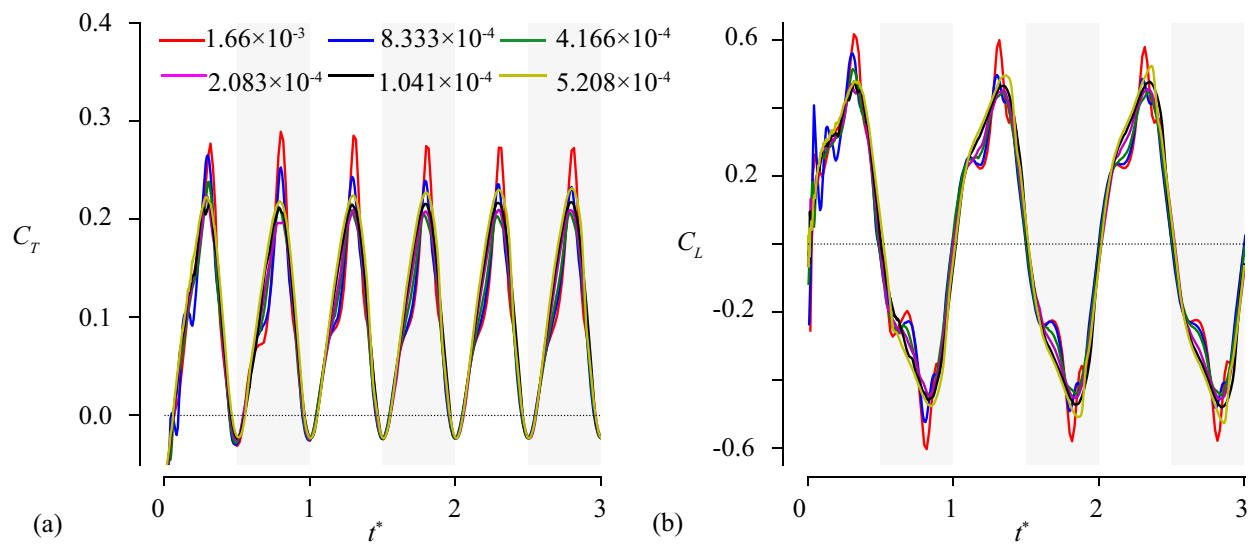


Fig. B2. Timestep sensitivity results with the baseline grid for six different timesteps. Time history of (a) thrust and (b) lift coefficients for three flapping cycles.

Table B2. Timestep sensitivity results for the baseline grid. The norms for  $C_L$  and  $C_T$  are calculated between  $t^* = 2$  and  $t^* = 3$ . The  $L_1$  and  $L_2$  norms are normalized with the timestep per cycle [35].

Timesteps Per cycle	Timestep $\Delta t$ (s)	$C_{ m L}$			$C_{\mathrm{T}}$		
		$L_1$ norm	$L_2$ norm	$L_{\infty}$ norm	$L_1$ norm	$L_2$ norm	$L_{\infty}$ norm
60	1.66×10 <sup>-3</sup>	0.0783	0.0873	0.179	0.0298	0.0365	0.09
120	$8.333 \times 10^{-4}$	0.0663	0.0737	0.119	0.0237	0.0292	0.062
240	$4.166 \times 10^{-4}$	0.0535	0.0583	0.116	0.0204	0.0247	0.05
480	$2.083 \times 10^{-4}$	0.0314	0.0369	0.085	0.0133	0.0171	0.039
960 (baseline)	$1.041 \times 10^{-4}$	0.0202	0.0248	0.063	0.0078	0.0101	0.024
1920	$5.208 \times 10^{-5}$	-	-	-	-	-	_

#### References

- [1] Merlin, C., Gegear, R. J., and Reppert, S. M., "Antennal Circadian Clocks Coordinate Sun Compass Orientation in Migratory Monarch Butterflies," *Science*, Vol. 325, Nr. September, 2009, pp. 1700–1705.
- [2] Brower, L. P., Fink, L. S., and Walford, P., "Fueling the Fall Migration of the Monarch Butterfly," *Integrative and Comparative Biology*, Vol. 46, Nr. 6, 2006, pp. 1123–1142.
- [3] Brower, L., "Monarch Butterfly Orientation: Missing Pieces of a Magnificent Puzzle," *Journal of Experimental Biology*, Vol. 199, Nr. 1, 1996, pp. 93–103.
- [4] Gibo, D. L., "Altitudes Attained by Migrating Monarch Butterflies, Danaus Plexippus (Lepidoptera: Danainae), as Reported by Glider Pilots," *Canadian Journal of Zoology*, Vol. 59, Nr. 3, 1981, pp. 571–572.
- [5] Taylor, L. R., "Insect Migration, Flight Periodicity and the Boundary Layer," *Journal of Animal Ecology*, Vol. 43, Nr. 1, 1974, pp. 225–238.
- [6] Gibo, D. L., and Pallet, M. J., "Soaring Flight of Monarch Butterflies, Danaus Plexippus (Lepidoptera: Danaidae), During the Late Summer Migration in Southern Ontario," *Canadian Journal of Zoology*, Vol. 57, Nr. 7, 1979, pp. 1393–1401.
- [7] Paoletti, P., and Mahadevan, L., "Intermittent Locomotion as an Optimal Control Strategy," *Proceedings of the Royal Society A: Mathematical, Physical and Engineering Sciences*, Vol. 470, 2014, p. 20130535.
- [8] Kovac, M., Vogt, D., Ithier, D., Smith, M., and Wood, R., "Aerodynamic Evaluation of Four Butterfly Species for the Design of Flapping-Gliding Robotic Insects," *IEEE International Conference on Intelligent Robots and Systems*, 2012, pp. 1102–1109.
- [9] Wassenaar, L. I., and Hobson, K. A., "Natal Origins of Migratory Monarch Butterflies at Wintering Colonies in Mexico: New Isotopic Evidence," *Proceedings of the National Academy of Sciences of the United States of America*, Vol. 95, Nr. 26, 1998, pp. 15436–15439.
- [10] Slayback, D. A., Brower, L. P., Ramirez, M. I., and Fink, L. S., "Establishing the Presence and Absence of Overwintering Colonies of the Monarch Butterfly in Mexico by the Use of Small Aircraft," *American Entomologist*, Vol. 53, Nr. 1, 2007, pp. 28–40.
- [11] Alonso-Mejía, A., Rendon-Salinas, E., Montesinos-Patiño, E., and Brower, L. P., "Use of Lipid Reserves by Monarch Butterflies Overwintering in Mexico: Implications for Conservation," *Ecological Applications*, Vol. 7, Nr. 3, 1997, pp. 934–947.
- [12] Urquhart, F. A., "Found at Last; the Monarch's Winter Home," *National Geographic Magazine*, Vol. 150, 1976, pp. 161–173.
- [13] Urquhart, F. A., and Urquhart, N. R., "The Overwintering Site of the Eastern Population of the Monarch Butterfly (Danaus Plexippus; Danaidae) in Southern Mexico," *Journal of the Lepidopterists' Society*, Vol. 30, Nr. 3, 1976, pp. 153–158.
- [14] Masters, A. R., Malcolm, S. B., and Brower, L. P., "Monarch Butterfly (Danaus Plexippus) Thermoregulatory Behavior and Adaptations for Overwintering in Mexico," *Ecology*, Vol. 69, Nr. 2, 1988, pp. 458–467.
- [15] NASA Technical Report, "U.S. Standard Atmosphere," NASA-TM-X-74335, 1976.
- [16] Twigg, R., Sridhar, M. K., Pohly, J. A., Hilderbrant, N., Kang, C., Landrum, D. B., Roh, K.-H., and Salzwedel, S., "Aeroelastic Characterization of Real and Artificial Monarch Butterfly Wings," AIAA Scitech Forum, Orlando, FL: AIAA 2020-2002, 2020.
- [17] Combes, S. A., and Daniel, T. L., "Flexural Stiffness in Insect Wings. I. Scaling and the Influence of Wing Venation.," The Journal of experimental biology, Vol. 206, Nr. Pt 17, 2003, pp. 2979–2987.
- [18] Mountcastle, A. M., Combes, S. a, and Mountcastle, A. M., "Wing Flexibility Enhances Load-Lifting Capacity in Bumblebees.," *Proceedings. Biological Sciences / The Royal Society*, Vol. 280, Nr. 1759, 2013, p. 20130531.
- [19] Eldredge, J. D., Toomey, J., and Medina, A., "On the Roles of Chord-Wise Flexibility in a Flapping Wing with Hovering Kinematics," *Journal of Fluid Mechanics*, Vol. 659, 2010, pp. 94–115.
- [20] Ramananarivo, S., Godoy-Diana, R., and Thiria, B., "Rather than Resonance, Flapping Wing Flyers May Play on

- Aerodynamics to Improve Performance," *Proceedings of the National Academy of Sciences*, Vol. 108, Nr. 15, 2011, pp. 5964–5969.
- [21] Vanella, M., Fitzgerald, T., Preidikman, S., Balaras, E., and Balachandran, B., "Influence of Flexibility on the Aerodynamic Performance of a Hovering Wing.," *The Journal of Experimental Biology*, Vol. 212, Nr. Pt 1, 2009, pp. 95–105.
- [22] Kang, C., Aono, H., Cesnik, C. E. S., and Shyy, W., "Effects of Flexibility on the Aerodynamic Performance of Flapping Wings," *Journal of Fluid Mechanics*, Vol. 689, 2011, pp. 32–74.
- [23] Walker, S. M., Thomas, A. L. R., and Taylor, G. K., "Deformable Wing Kinematics in Free-Flying Hoverflies.," *Journal of the Royal Society, Interface / the Royal Society*, Vol. 7, Nr. 42, 2010, pp. 131–142.
- [24] Young, J., Walker, S. M., Bomphrey, R. J., Taylor, G. K., and Thomas, A. L. R., "Details of Insect Wing Design and Deformation Enhance Aerodynamic Function and Flight Efficiency.," *Science*, Vol. 325, Nr. 5947, 2009, pp. 1549– 1552.
- [25] Nakata, T., and Liu, H., "Aerodynamic Performance of a Hovering Hawkmoth with Flexible Wings: A Computational Approach," *Proceedings of the Royal Society B: Biological Sciences*, Vol. 279, Nr. 1729, 2012, pp. 722–731.
- [26] Sridhar, M., Kang, C.-K., Landrum, D. B., and Aono, H., "Fluid-Structure Interaction of Flexible Flapping Wings at High Altitude Conditions," AIAA Scitech 2020 Forum, Orlando, FL: AIAA 2020-1781, 2020.
- [27] Shyy, W., Aono, H., Chimakurthi, S. K., Trizila, P., Kang, C. K., Cesnik, C. E. S., and Liu, H., "Recent Progress in Flapping Wing Aerodynamics and Aeroelasticity," *Progress in Aerospace Sciences*, Vol. 46, Nr. 7, 2010, pp. 284–327.
- [28] Chimakurthi, S. K., Tang, J., Palacios, R., S. Cesnik, C. E., and Shyy, W., "Computational Aeroelasticity Framework for Analyzing Flapping Wing Micro Air Vehicles," *AIAA Journal*, Vol. 47, Nr. 8, 2009, pp. 1865–1878.
- [29] Bluman, J., and Kang, C. K., "Wing-Wake Interaction Destabilizes Hover Equilibrium of a Flapping Insect-Scale Wing," *Bioinspiration and Biomimetics*, Vol. 12, Nr. 4, 2017.
- [30] Bluman, J., and Kang, C., "Achieving Hover Equilibrium in Free Flight with a Flexible Flapping Wing," *Journal of Fluids and Structures*, Vol. 75, 2017, pp. 117–139.
- [31] Bluman, J. E., Sridhar, M. K., and Kang, C., "Chordwise Wing Flexibility May Passively Stabilize Hovering Insects," *Journal of Royal Society Interface*, Vol. 15, 2018, p. 20180409.
- [32] Twigg, R., "Aeroelastic Characerization of Real and Bioinspired Artificial Butterfly Wings," Msc. Thesis, The University of Alabama in Huntsville, 2020.
- [33] Shyy, W., Aono, H., Kang, C., and Liu, H., An Introduction to Flapping Wing Aerodynamics, New York: Cambridge University Press, 2013.
- [34] de Boer, A., van der Schoot, M. S., and Bijl, H., "Mesh Deformation Based on Radial Basis Function Interpolation," Computers and Structures, Vol. 85, Nr. 11–14, 2007, pp. 784–795.
- [35] Roy, C. J., "Grid Convergence Error Analysis for Mixed-Order Numerical Schemes," AIAA Journal, Vol. 41, Nr. 4, 2003.